RESEARCH ARTICLE

Angiogenesis in Free-Standing Two-Vasculature-Embedded Scaffold Extruded by Two-Core Laminar Flow Device

Chanh Trung Nguyen[1], Van Thuy Duong[1], Chang Ho Hwang[2], Kyo-in Koo[1]*

[1]Major of Biomedical Engineering, Department of Electrical, Electronic and Computer Engineering, University of Ulsan, Ulsan, Republic of Korea
[2]Department of Physical and Rehabilitation Medicine, Chungnam National University Sejong Hospital, College of Medicine, Chungnam National University, Sejong, Republic of Korea

Abstract: Rapid construction of pre-vascular structure is highly desired for engineered thick tissue. However, angiogenesis in free-standing scaffold has been rarely reported because of limitation in growth factor (GF) supply into the scaffold. This study, for the 1st time, investigated angiogenic sprouting in free-standing two-vasculature-embedded scaffold with three different culture conditions and additional GFs. A two-core laminar flow device continuously extruded one vascular channel with human umbilical vein endothelial cells (HUVECs) and a 3 mg/ml type-1 collagen, one hollow channel, and a shell layer with 2% w/v gelatin-alginate (70:30) composite. Under the GF flowing condition, angiogenic sprouting from the HUVEC vessel had started since day 1 and gradually grew toward the hollow channel on day 10. Due to the medium flowing, the HUVECs showed elongated spindle-like morphology homogeneously. Their viability has been over 80% up to day 10. This approach could apply to vascular investigation, and drug discovery further, not only to the engineered thick tissue.

Keywords: Angiogenesis; Pre-vascularized tissue; Two-core vasculature; Gelatin-alginate; Free standing; Culture condition

***Correspondence to:** Kyo-in Koo, Major of Biomedical Engineering, Department of Electrical, Electronic and Computer Engineering, University of Ulsan, Nam-gu, Ulsan 44610, Republic of Korea; kikoo@ulsan.ac.kr

Received: January 19, 2022; **Accepted:** April 1, 2022; **Published Online:** May 13, 2022

Citation: Nguyen CT, Duong VT, Hwang CH, *et al.*, 2022, Angiogenesis in Free-Standing Two-Vasculature-Embedded Scaffold Extruded by Two-Core Laminar Flow Device. *Int J Bioprint,* 8(3):557. http://doi.org/10.18063/ijb.v8i3.557

1. Introduction

The vascular network densely permeates organs to provide efficient mass transfer in body[1]. These branched vessels transfer nutrients and oxygen and withdraw metabolic waste from organs[2]. The functioning vascular network is essential as well when creating engineered thick tissue. In *in vivo* environment, cells are generally located within less than 200 μm from blood vessels to avoid ischemic conditions[3]. However, fabricated tissue *in vitro* lacked the vasculature network so that cells inside the engineered tissue often received nutrients by diffusion over 200 μm, at the worst case over 1 mm[4].

To fabricate pre-vasculature channels, various methods including electrospinning[5], molding[6], laser degradation[7], co-axial extruding[8-10], acoustofluidic extruding[11], cell sheet stacking[12], and cell coculture[13] have been proposed. These approaches have demonstrated their achievement but still require more development because prolonged fabrication time and complex manual processes can damage cell viability. In addition, limited vasculature layer number and complex fabrication process of mesovasculatures are other challenges that need to be tackled[14].

Therefore, not only the pre-vascularizing method but also a method for easy angiogenesis is required for the engineered thick tissue. Some angiogenesis process inside a microfluidic chip has been investigated[15-17]. However, angiogenesis in free-standing scaffolds has been rarely reported because supplying growth factor (GF) or implementing GF gradient inside the 3D scaffolds is not easy. Couple of reports demonstrated angiogenesis with a single-channel structure. Duong *et al.* extruded the double-layered single-vascular scaffold with human umbilical vein endothelial cell (HUVEC) and human aortic smooth muscle cell (HASMC)[18]. In their

investigation, the GF secreted from the HASMC layer-induced angiogenic sprouting. Gao *et al.* fabricated HUVEC single-layered single-vascular scaffold and demonstrated angiogenic sprouting using GF mixed collagen[19]. These methods were not appropriate for vascular network of the engineered thick tissue.

In this study, we extruded two-vasculature-embedded scaffold and demonstrated angiogenesis for the pre-vascularized tissue. The structure of scaffold consisted of one hollow channel for flowing GF mixed media and one HUVEC core for a vascular channel (**Figure 1**). GF gradient from the hollow channel induced angiogenic sprouting from the HUVEC vessel inside the generated scaffold. This angiogenesis was compared at three different culture conditions and analyzed quantitatively. Effect of shear stress, perfusibility, cell viability, and core size were also evaluated.

2. Materials and methods

2.1. Two-core laminar flow device

A two-core laminar flow device was designed and fabricated based on our previous device (**Figure 2**)[20]. It has three inner glass capillaries (580 μm inner diameter [ID], G100-3, Warner Instruments LLC, U.S.A.) for inlets and one outer glass capillary (1160 μm internal diameter, G200-3, Warner Instruments LLC, U.S.A.) for an outlet. Two glass tubes among the three 580 μm ID tubes were tapered as approximately 200 μm using a puller (PC-10, Narishige, Japan) for the two inner core inlets. The other 580 μm ID tube supplied the outmost layer material to the 1160 μm ID tube without any tapering. All the four tubes linked each other in a block of polydimethylsiloxane (PDMS, Dow Corning Corporation, U.S.A.). The fabricated device was sterilized at 121°C for 15 min before biological experiments.

2.2. HUVEC culture

HUVEC was purchased from the American Type Culture Collection (ATCC, U.S.A.) and cultured in vascular cell basal medium (ATCC, U.S.A.) supplemented with Endothelial Cell Growth Kit-VEGF (ATCC, U.S.A.). Media were changed 3 times a week. They were cultured in a humidified incubator at 37°C with 5% CO_2 and were passaged before reaching approximately 80% surface coverage. The cells within passage from 10 to 15 were used in experiments.

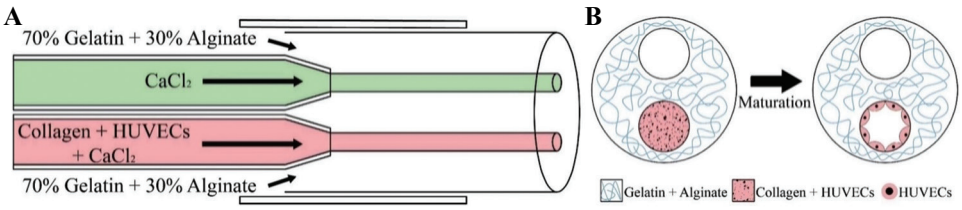

Figure 1. The schematic of the two-vasculature-embedded scaffold. (A) One core (the green one) consisted of 0.1 M calcium chloride dihydrate ($CaCl_2$) only for the hollow channel. Another core (the pink one) was made of HUVECs, 3 mg/mL type-1 collagen, and 0.1 M $CaCl_2$ for the vascular channel. The shell layer consisted of gelatin and sodium alginate. (B) The cross-sectional view of the two-vasculature-embedded scaffold right after the formation and after the maturation.

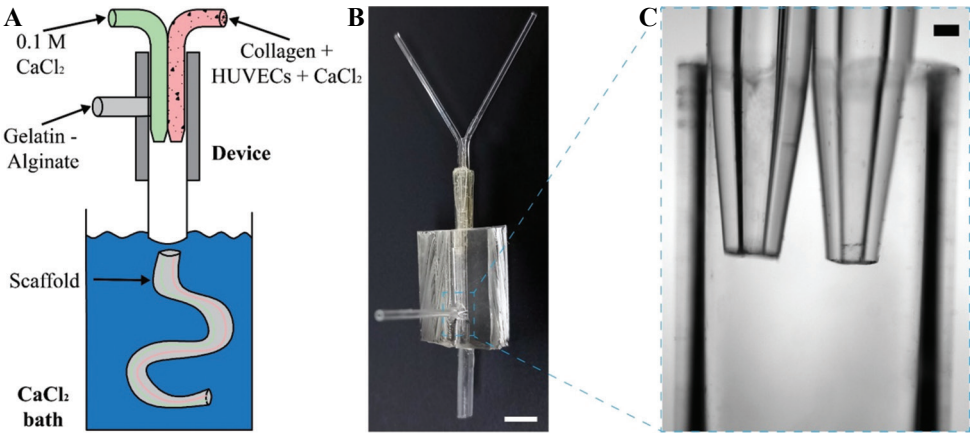

Figure 2. The two-core laminar flow device; (A) the schematic of the two-core laminar flow device and the $CaCl_2$ bath; (B) the fabricated device (scale bar: 5 mm); (C) the microscope image of the two-core area among two inlet glasses and the body glass (scale bar: 200 μm).

2.3. Two-vasculature-embedded scaffold formation

Three syringe pumps (11 Elite C300918, Harvard Apparatus, U.S.A.) were connected to the fabricated device through Tygon tubes (Saint-Gobain, Courbevoie, France). For one core inlet, a mixture of 3 mg/mL collagen, 2 × 10^6 cells/mL HUVECs, and 0.1 M $CaCl_2$ (Daejung Chemicals, Republic of Korea) was supplied to culture into a blood vessel. For another core inlet, 0.1 M $CaCl_2$ was injected to formulate a hollow channel inside the scaffold. For the outer layer inlet, a 2% w/v mixture of gelatin (Sigma-Aldrich, U.S.A.) and alginate (Daejung Chemicals, Republic of Korea) (70 vs. 30 ratio) was supplied as the body of the scaffold. The extruded scaffold was submerged into a 0.1 M $CaCl_2$ bath through the outlet and then cross-linked. Calcium ions of the $CaCl_2$ cross-linked with sodium alginate into calcium alginate so that no hydrogel in the hollow channel remained. The gelatin scaffold was washed with phosphate-buffered saline (PBS, Sigma-Aldrich, U.S.A.). The washed scaffold was cultured in an incubator at 37°C with 5% CO_2 and replaced with a fresh medium every 2 days.

2.4. Laboratory made connecting device

A connecting device was fabricated to link a syringe pump to the generated scaffold (**Figure 3** and **Figure S1**). First, a 2.0 mm ID glass tube and a Pasteur pipette (Hilgenberg, Germany) were cut and then bonded using PDMS (**Figure 3A**). A hole was punched at a Petri dish (SPL, Republic of Korea). The attached glass holder was fixed at the hole punched Petri dish using PDMS (**Figure 3B**). After checking no leakage, the fabricated connecting device was sterilized with 99.9% ethanol in 24 h for biological experiments.

2.5. Three types of culture condition

The formulated two-vasculature-embedded scaffolds were cultured in three different conditions: (i) Obstructing media diffusion by a glass tube; (ii) soaking in a media dish; and (iii) flowing media inside the two-vasculature-embedded scaffold, as shown in **Figure 4**.

To hinder media diffusion inside the formulated scaffold, it was inserted into a glass tube and then immersed in culture media. The glass tube has a tapered structure with about 1000 μm ID at one end and about 2000 μm ID at the other end. Using a syringe pump, the 1000 μm outer diameter (OD) scaffold was sucked and fixed into the narrow end of the tapered tube. The scaffold was fixed in the tapered glass tube soaked in culture media. To make conventional media diffusion condition into the embedded cells, the generated scaffold was just soaked in culture media. To supply culture media through the hollow channel of the generated scaffold, one end of the generated scaffold was sucked and fixed at the holder of the laboratory made connecting device. Alginate was used to fill the gap between the holder and the fixed scaffold for a secure connection. Culture media were provided at a flow rate of 10 μL/min from a syringe pump to the connected scaffold and then flowed out the not connected end of the scaffold. At the initial status of the media supply, there have been no culture media out of the scaffold. However, as culture media flowed out continuously, the dumped media made a puddle around the scaffold. The media puddle trashed out of the Petri dish every 24 h.

2.6. Diffusion from the hollow channel

To select flow rate inside the hollow channel of the generated scaffold, the cell-free two-vasculature-embedded scaffold was produced, and red food dye flowed through the cell-free scaffold from 2 μL/min to 20 μL/min. Using a bright-field microscope, the diffusion rate and morphology of the red food dye were observed. Based on the food dye diffusion observation, flow and diffusion of green fluorescence dye in PBS (1:1000) were analyzed quantitatively using a fluorescence microscope.

2.7. Perfusibility in the two vasculatures

Blue fluorescence microbeads (5.42 μm ± 0.09 μm, GmbH, Germany) in PBS (1:200) were flowed to check the perfusibility of the HUVEC vessel. To develop the HUVEC-collagen core into the blood vessel, the formulated scaffold was cultured in the soaking condition for 2 days. After 2-day maturing, Calcein AM dye (Thermo Scientific, U.S.A.) stained alive cells to distinguish the HUVEC vessel from the hollow channel. The green

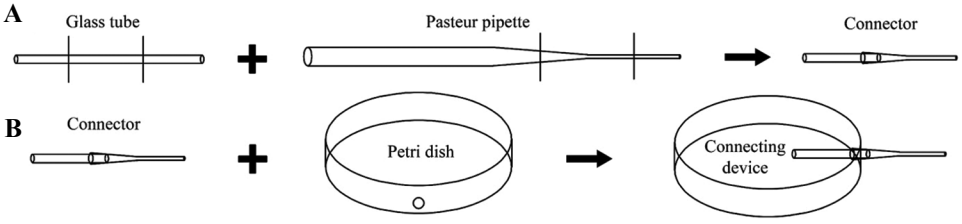

Figure 3. The fabrication process of the connecting device. (A) The holder fabrication process. (B) The attaching process of the hole punched Petri dish and the holder.

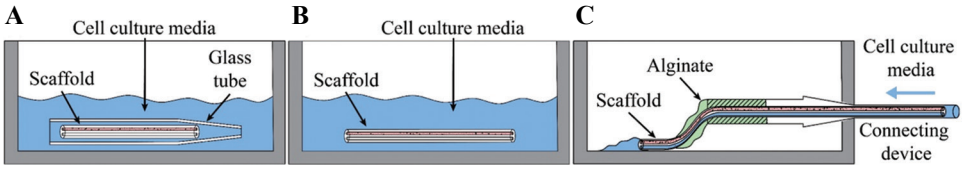

Figure 4. The three types of culture conditions. (A) The obstructing condition. (B) The soaking condition. (C) The flowing condition.

stained scaffold was linked to a syringe pump using the laboratory made connecting device, and then, the syringe pump flowed the blue fluorescence microbeads to the green stained scaffold.

2.8. GFs for angiogenic sprouting

To observe angiogenic sprouting, additional GFs were injected into the growth kit added medium, following the previous studies[15,21]. The concentration of the additional GFs was 50 ng/mL of vascular endothelial GF (Preprotech, U.S.A.), 50 ng/mL of basic fibroblast GF (Preprotech, U.S.A.), and 50 ng/mL of hepatocyte GF (Preprotech, U.S.A.). For the first 2 days, the generated scaffolds have been cultured in the growth kit added media only to develop vascular structure. Since day 3, the additional GF was provided and changed every 2 days.

2.9. Staining for viability analysis

Viability and proliferation of the HUVEC inside the formulated scaffold were evaluated at days 1, 3, 5, 7, and 10 in all three culture conditions with and without GFs using live/dead viability kit for mammalian cells (L3224, Thermo Scientific, U.S.A.). Its concentration was 0.05% of Calcein AM (4 mM) in anhydrous dimethyl sulfoxide (DMSO) and 0.2% ethidium homodimer-1 (2 mM) in DMSO/H_2O at 1:4 (v/v). The stained scaffold was washed 3 times in PBS and then observed under a fluorescent microscope.

Fluorescent intensity of live cells (green channel) and dead cells (red channel) was analyzed by ImageJ software (Fiji, NIH Image, U.S.A.). Percentage of the cell viability was calculated using a ratio between the green intensity and summation of the green and red intensity.

$$\text{Cell viability} = \frac{\text{Green intensity}}{\text{Green intensity} + \text{red intensity}} \times 100 \quad (1)$$

2.10. Immunofluorescent staining

To observe migration, morphology, and angiogenesis of the embedded HUVEC, F-actin, CD31, and nuclei were stained using rhodamine-phalloidin, anti-CD31, and DAPI, respectively. First, the formulated scaffold was fixed with 4% paraformaldehyde (P6148, Sigma-Aldrich, U.S.A.) for 40 min at room temperature (RT). The fixed scaffold was immersed in alginate lyase (Sigma-Aldrich, U.S.A.) solution to remove alginate at 37°C. The alginate removed HUVEC core was immersed in a collagen matrix and incubated at 37°C for gelation. Subsequently, the HUVEC core in collagen was permeabilized with 0.1% Triton X-100 (Sigma-Aldrich, U.S.A.) for 5 min at RT. Primary antibody of anti-CD31 (MA5-13188, Invitrogen, U.S.A.) was incubated at 4°C overnight. Then, secondary antibodies (Alexa Fluor 488, Invitrogen, U.S.A.) and Phalloidin (Alexa Fluor 488, Invitrogen, U.S.A.) were applied for 2 h at RT. Besides, nuclei of the HUVEC core were stained with DAPI (D1396, Invitrogen, U.S.A.) for 5 min. After every chemical treating step, the treated sample was washed 3 times with PBS for 5 min. The stained samples were observed using an IX53 inverted fluorescent microscope (Olympus, Japan) and a FV1000 laser scanning confocal microscope (Olympus, Japan).

2.11. Statistical analysis

The result was represented with a mean value ± one standard error from three independent repetitions. To evaluate the statistical significance level, one-way ANOVA and Tukey's *post hoc* test were utilized. Its significance is remarked as * for $P < 0.05$, ** for $P < 0.01$, and *** for $P < 0.001$.

3. Results

3.1. Fabrication of the two-vasculature-embedded scaffold

The two-vasculature-embedded scaffolds without cells were controllably and continuously generated using our two-core-embedded device. After complete gelation, the fabricated scaffolds were uniform and stable with a length of meters (**Figure 5A**). Various flow rates of the gelatin-alginate fluid, the collagen-$CaCl_2$ fluid, and the $CaCl_2$ fluid were explored to select diameters of the shell and two vasculatures for further experiments. In **Figure 5C**, the graph presented scaffolds' diameter with respect to the shell flow rate at a fixed core flow rate of 0.1 mL/min. As the shell flow rate increased from 1.5 mL/min to 3 mL/min, the shell diameter increased from 948 μm to 1095 μm. Besides, the diameter of the collagen core decreased from 376 μm to 262 μm, and that of the $CaCl_2$ core also decreased from 331 μm to 203 μm. In addition to the shell flow rate change, the core flow rate

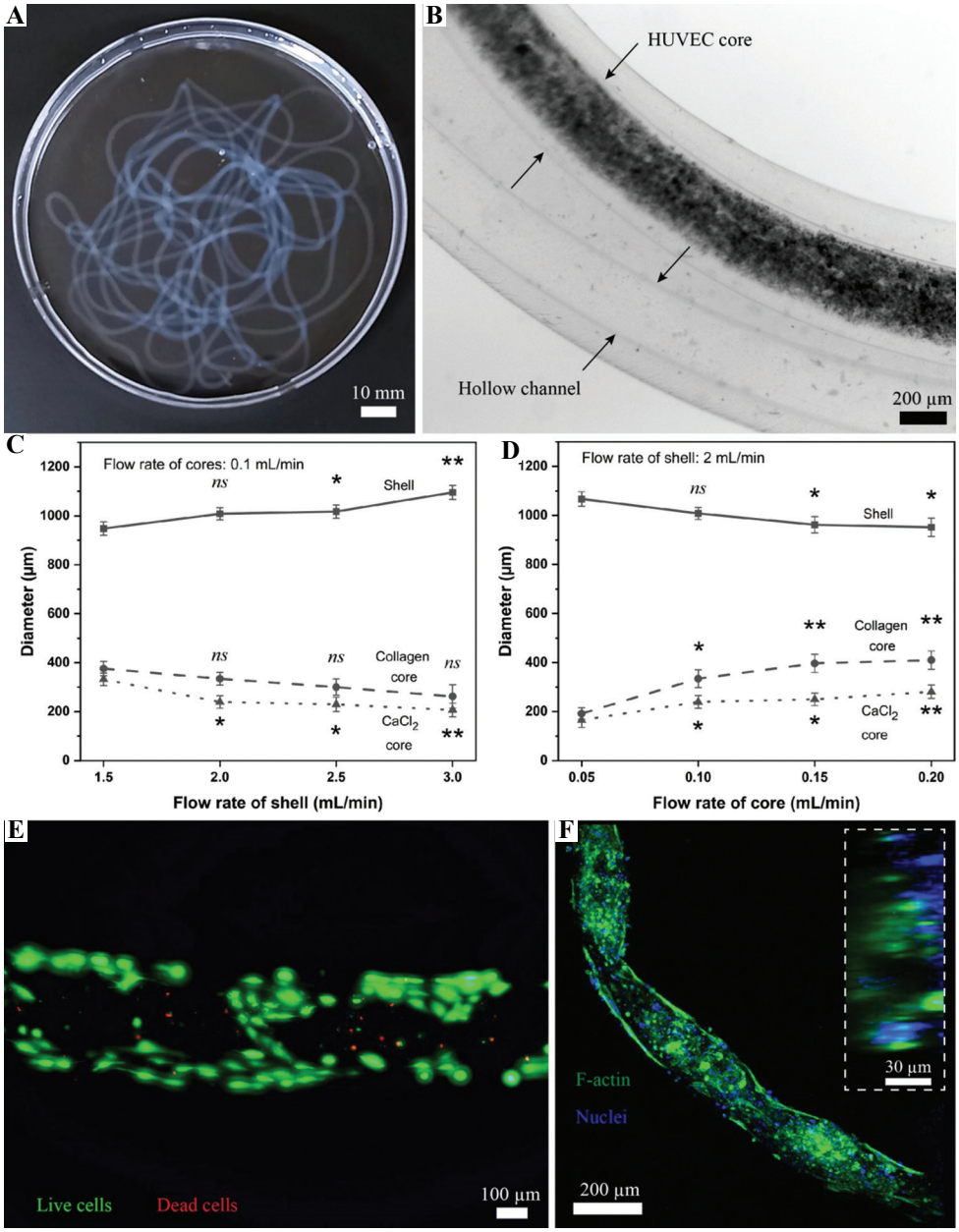

Figure 5. The fabricated two-vasculature-embedded scaffold; (A) the generated scaffold in the Petri dish after the formation (scale bar: 10 mm); (B) The bright-field microscope images of the scaffold with the HUVEC core and the hollow channel after the formation (scale bar: 200 μm); (C) The diameter of the shell and the two channels with the flow rate of the cores as 0.1 mL/min and various flow rates of the shell; (D) the diameter of the shell and the cores with the flow rate of the shell as 2 ml/min and various flow rates of the cores; (E) the fluorescent image of the stained HUVECs inside the fabricated scaffold after 1-day culture (scale bar: 100 μm). (F) The confocal image of the HUVECs after 2-day culture (scale bar: 200 μm) and the cross-sectional view of the lumen structure in the HUVECs (scale bar: 30 μm).

shift was also investigated. The shell diameter decreased from 1067 μm to 951 μm in an increment of the core flow rate from 0.05 mL/min to 0.2 mL/min when the shell flow rate was constant with 2 mL/min (**Figure 5D**). The diameter of the collagen core and $CaCl_2$ core increased from 191 μm to 409 μm and from 165 μm to 281 μm, respectively. Therefore, the shell flow rate with alginate-gelatin mixture as 2 mL/min and the two-core flow rate with collagen, HUVEC, and $CaCl_2$ as 0.1 mL/min were designated to fabricate two-vasculature-embedded scaffolds for experiment with cells.

Figure 5B shows the formulated two-vasculature-embedded scaffold under the bright-field microscope. Two separated cores with a transparent hollow channel and a HUVEC filled channel were observed. Aggregation of individual cells at day 0 (**Figure 5B**) has gradually

stretched, migrated, and connected to produce ECs' networks after 1 day of culture (**Figure 5E**). Confocal images of the HUVEC core exhibited a hollow center in cross-section view (**Figure 5F**). HUVEC has the propensity to form luminal structures in the three-dimensional matrix[22], which can be perfused[18,22,23].

3.2. Perfusability

To optimize flow rate through the hollow channel, the red dye has flowed through the hollow channel of the cell-free two-vasculature-embedded scaffold, as shown in **Figure 6**. The flow rates over 10 μL/min have diffused into all parts of the scaffold in 10 min. However, 2 μL/min and 5 μL/min required 15 min for the entire diffusion. Even though it diffused at all parts of the scaffold, its color gradient differed according to the flow rate. As the flow rate increased, its red color became deep in less time. However, in our previous study[24,25], the flow rate over 20 μL/min has made the linking part from the connecting device to the scaffold loosen in a short time. Therefore, 10 μL/min was selected for the secure connection in this investigation.

Fluorescence fluid was also pumped into the hollow channel with the flow rate of 10 μL/min until 60 min to understand diffusion in our scaffold. **Figure 7** presented the temporal sequence of the fluorescence microscope images. Based on the temporal images, fluorescence intensity was analyzed. The most gray value at 1 time point showed an increasing tendency as time went (**Figure 7B**). The integrated density exhibited a similar tendency with the most gray value (**Figure 7C**). Considering these two graphs, 15 min was a meaningful time to diffuse significantly up to about 100 μm apart from the edge of the channel.

Perfusibility of the HUVEC vessel was evaluated with blue fluorescence microbead, as shown in **Figure 8** and **Supplementary Video**. The blue fluorescence microbead flowed continuously in the HUVEC vessel. It showed that the embedded HUVECs have well developed into the vascular structure. Even though the syringe pump drove the blue microbead identically to both channels at the flow rate of 10 μL/min, the hollow channel flowed much more microbeads than the HUVEC vessel (**Figure 8B**). It was presumed that the HUVEC vessel had much more bumpy structures than the hollow channel for the microbead to pass through.

3.3. Cell morphology according to the culture condition

Different F-actin expression of the embedded HUVECs was observed according to the culture condition, as shown in **Figure 9**. The cells in the obstructing condition exhibited arbitrary size and cobblestone-like morphology with random orientation (**Figure 9A**). The soaking condition showed spindle-like morphology doped in the cobblestone-like morphology with random orientation (**Figure 9B**). Particularly, the cells in the flowing condition presented uniform spindle-like morphology with the arrangement in the flow direction (**Figure 9C**). These results indicated that cell elongation and alignment of the flowing condition are similar *in vivo*[26]. For further quantitative analysis, three morphometric parameters of the embedded HUVECs, namely, perimeter, elongation ratio, and orientation deviation (**Figure 9D-F**), were

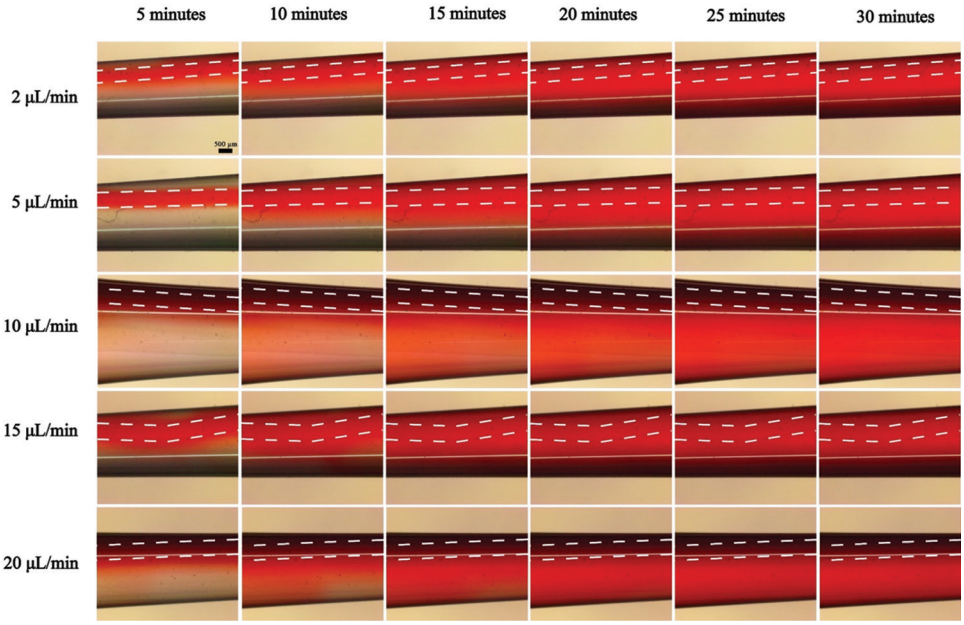

Figure 6. The time-lapse images of the perfused channel from 5 min to 30 min at various flow rates (scale bar: 1 mm).

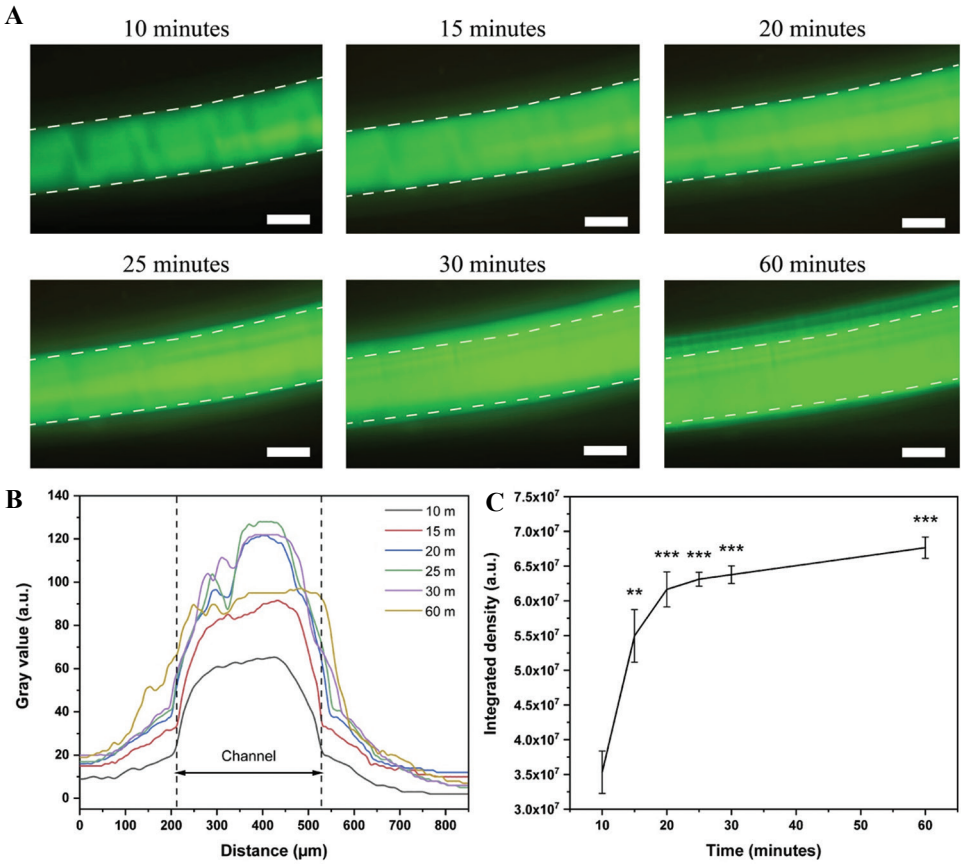

Figure 7. The perfusion assay; (A) the time-lapse fluorescence images of the channel from 0 min to 60 min at 10 μL/min of fluorescence fluid (scale bar: 200 μm). (B) The fluorescent intensity profile in the channel was graphed according to the distance. (C) The integrated density was analyzed with respect to the time.

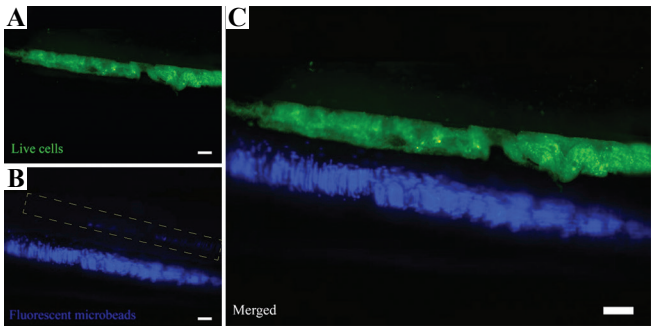

Figure 8. The fluorescence images of the two-vasculature-embedded scaffold during pumping; (A) the fluorescence images of the live-/dead-stained HUVEC channel. (B) The hollow channel with the blue fluorescent microbeads. (C) The fluorescence images of the two vasculatures (green: Live cell, blue: Microbeads, scale bar: 200 μm).

investigated. The orientation deviation was calculated from the standard deviation of cell orientation, the direction of the longer part in the embedded HUVEC morphology. The cells in the flowing condition exhibited the longest perimeter, the highest elongation ratio, and the lowest orientation deviation. It means that the cells in the flowing condition were mostly elongated and aligned among three culture conditions.

3.4. Cell viability

Figures 10 and **11** showed the viability of the embedded HUVECs in the generated two-vasculature-embedded scaffold up to day 10. Until day 3, the cells were developed with uniform distribution in all three conditions (**Figure 10A** and **B**). Since day 5, the cells in the obstructing condition were shrunk comparing with the other conditions. These tendencies look similar in both cases of the GF and the non-GF.

Quantitative viability analysis explained more about the effect of the culture condition and the additional GFs. The cells in the obstructing condition have survived much less than the other conditions at any time point (**Figure 11A** and **B**). They looked dying. In the non-additional GFs case, the cells in the flowing condition (80.9%) exhibited slightly more viability than the cells in the soaking condition (76.9%) at day 10. In the additional GFs case, those in the flowing condition (78.4%) presented moderately less viability than those in

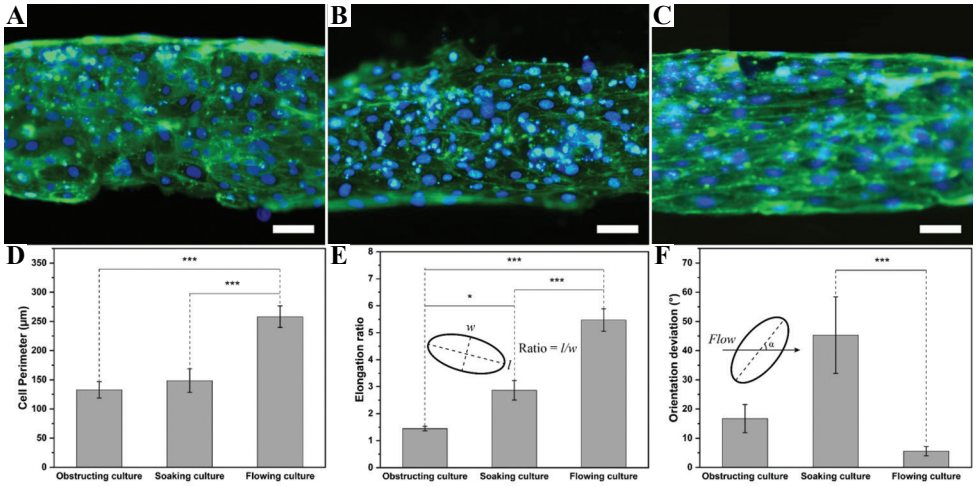

Figure 9. The morphology characterization in the HUVEC channel on day 2; the stained HUVECs in (A) the obstructing condition, (B) the soaking condition, and (C) the flowing condition (scale bar: 50 μm). The quantification of (D) the perimeter, (E) the elongation ratio, and (f) the orientation deviation of the stained HUVECs.

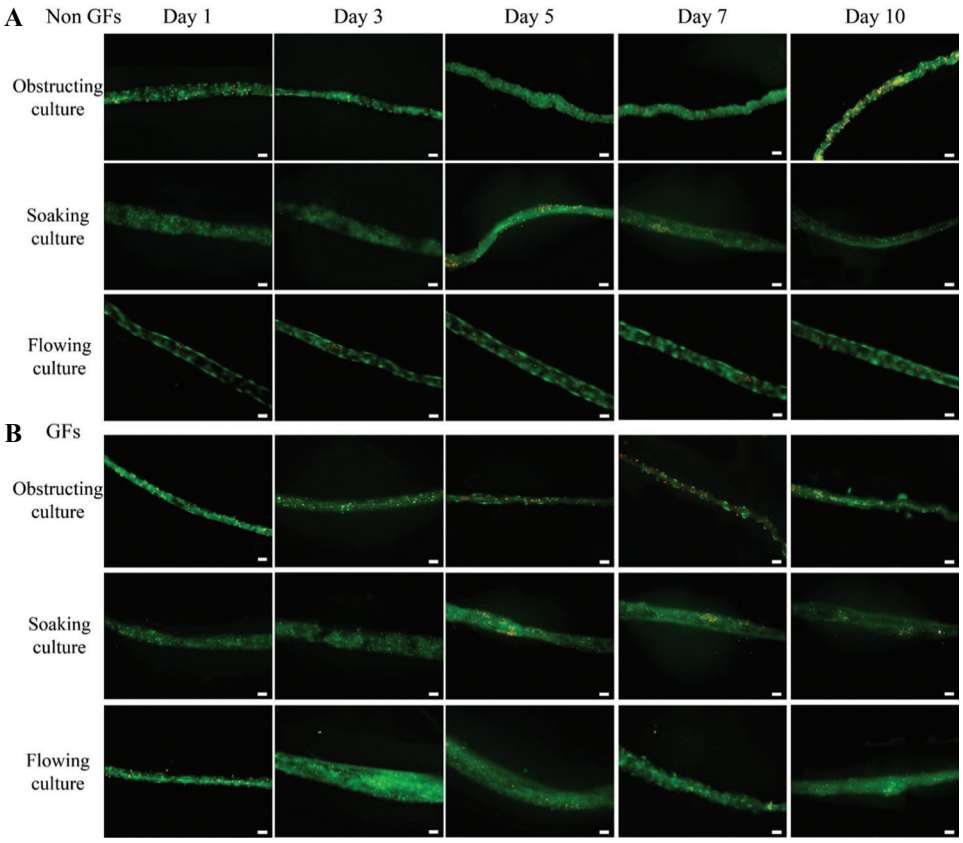

Figure 10. The fluorescence images of the live-/dead-stained HUVECs at the obstructing condition, the soaking condition, and the flowing condition (A) without the additional GFs and (B) with the additional GFs (scale bar: 200 μm).

the soaking condition (79.3%). However, they were not statistically different from each other.

The results indicated that the glass capillary of the obstructing condition restricted the medium diffusion into the embedded HUVECs. Right after generating the two-vasculature-embedded scaffold, the soaking condition caused only the formulated scaffold immediately submerge into media without any handling for connection, which was different from the other two conditions. It could make the

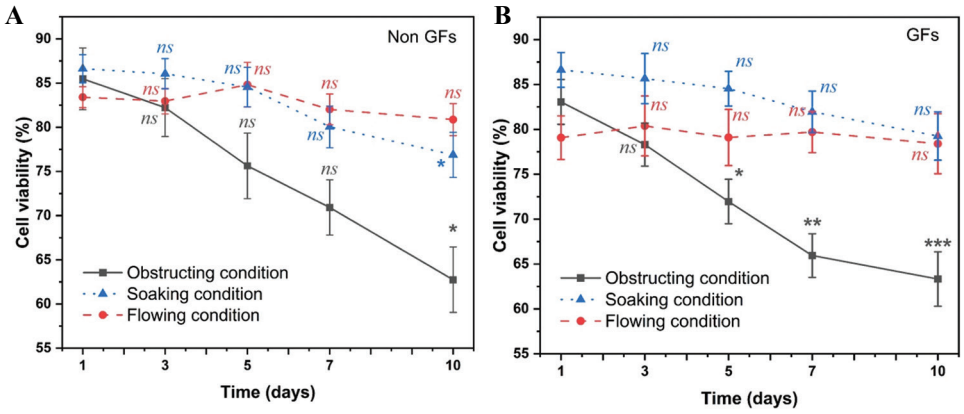

Figure 11. The cell viability of the two-vasculature-embedded scaffold according to the culture conditions (A) without the additional GFs and (B) with the additional GFs.

highest viability at day 0 and early days among all three culture conditions. The additional GFs did not significantly influence the cell viability in all three culture conditions.

3.5. Angiogenic sprouting

Figure 12 exhibited the angiogenic sprouting of the embedded HUVECs in the generated two-vasculature-embedded scaffold up to day 10 with F-actin (**Figure 12A-C**) and CD31 (**Figure 12D-F**) markers. The F-actin and CD31 are well-known biomarkers to check cytoskeleton and angiogenesis, respectively. The cells in the obstructing condition angiogenically sprouted from day 3 to day 7 (**Figure 12A** and **D**). Those sprouting looked no significant directionality. On day 10, all the sprouts disappeared, and no new sprouts were recognized. The cells in the soaking condition presented the angiogenic sprouting from day 3 to day 10 (**Figure 12B** and **E**). Considerate directionality was not observed as well. The cells in the flowing condition angiogenically sprouted during all the time points from day 1 to day 10 (**Figure 12C** and **F**). In particular, significant directionality of all the new sprouts to the hollow channel was observed, which diffused the high GF media into the HUVEC vessel. Furthermore, connections among adjacent sprouts were found on day 7 and day 10.

Sprouting number and length were quantitatively analyzed, as shown in **Figure 12D** and **E**. The flowing media inside presented an increasing tendency in both the number and the length. Except for the sprouting number at day 7, the cells in the flowing condition showed the highest number, the longest length among all the three conditions. On day 7, the sprouting number of the obstructing condition was slightly higher than that of the flowing condition. On day 7, the obstructing condition exhibited the highest number and the longest length among all the time points in the same culture condition. The sprouting number of the soaking condition showed the highest number at day 7 among all the time points in the same culture condition. In the case of the length, it presented a gradual increasing tendency.

The flowing condition showed the most active angiogenesis. It was assumed that the GF diffusion from the near hollow channel stimulated HUVECs more than the GF diffusion from the outside media. The glass capillary of the obstructing condition looked restricting the GF diffusion into the embedded HUVECs. It was demonstrated that below 65% cell viability in the obstructing condition could affect no angiogenesis at day 10.

4. Discussion

The formulated scaffolds consisted of two separated channels and the outer shell. One channel was filled with the mixture of HUVECs and type I collagen. The other channel was the hollow channel. The outer shell material was the composite of gelatin and alginate. The laboratory made connecting device linked the generated scaffold to a syringe pump for 10 days without any leakage. The flowed media diffused from the hollow channel to the embedded HUVECs. Due to the diffused media, aggregation of the individual HUVECs developed into the vascular structure. The angiogenic sprouting was induced from the HUVEC vessels to the hollow channel by the gradient of the additional GFs.

Scaffold material could be divided into natural, synthetic, hybrid, and decellularized extracellular matrix. Each group has its own advantages and disadvantages. Gelatin, a natural polymer, has been used in tissue engineering due to its high biocompatibility and biodegradability. However, the poor mechanical properties of gelatin restrict its application. Fortunately, alginate is generally used to improve its mechanical characteristics. Taking into consideration the previous investigations[27-29], the composite of gelatin-alginate

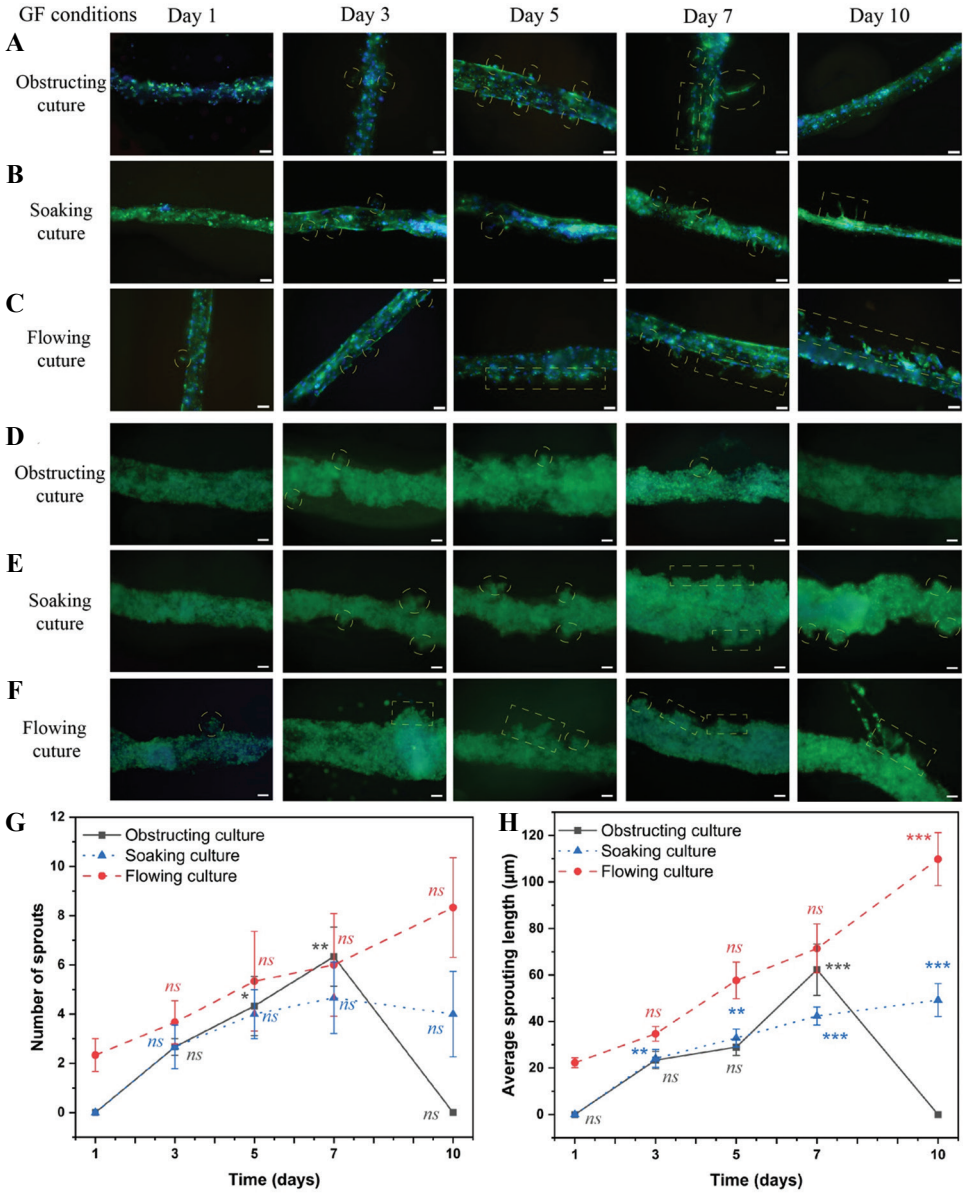

Figure 12. The angiogenic sprouting in all three culture conditions. The immunofluorescence images with F-actin signal of (A) the obstructing condition, (B) the soaking condition, and (C) the flowing condition (green: F-actin, blue: Nuclei, scale bar: 100 μm). The immunofluorescence images with CD31 signal of (D) the obstructing condition, (E) the soaking condition, and (F) the flowing condition (green: CD31, blue: Nuclei, scale bar: 100 μm). (G) The sprouting number was graphed. (H) The average length of the sprout was analyzed.

with weight ratio of 70:30 was chosen to enhance biocompatibility and mechanical properties.

In this study, the outer shell thickness and the distance between the two cores were approximately 280 – 290 μm and 140 – 150 μm, respectively. Rouwkema *et al.* demonstrated that cells show similar biological behavior at a distance <200 μm due to the supply of adequate culture medium by diffusion[30]. The maximum distance between capillaries is approximately 200 μm, usually <150 μm[31,32]. Therefore, our structure could be a potential model to investigate perfusion efficiency from one channel to another in a thick three-dimensional structure.

The hollow channel diameter could be adjustable in the range of approximately 200–400 μm (**Figure 4C** and **D**). This diameter corresponds to diameters of artery and vein[33]. The demonstrated angiogenic sprouting could be assumed as capillary network between artery and vein. Considering the previous investigations in **Table 1**, this study investigated relatively small diameter area.

The developed HUVEC vessel showed to flow microbeads (**Figure 8** and **Supplementary Video**). Lots

Table 1. The diameter and thickness of the fabricated scaffolds.

Cell sources	Inner diameter (mm)	Outer diameter (mm)	Wall thickness (mm)	References
Mesenchymal stem cells	4.0	5.5	0.75	[34]
Human smooth muscle cells	4.15		1.55	[35]
Fibroblast cells	0.55	0.61	0.1	[24]
Rat dermal fibroblasts		1.32		[36]
Human umbilical vein endothelial cells	2.5±0.5	8.7±0.5		[37]
Endothelial progenitor cells	4.75		0.4	[38]
Endothelial colony-forming cells	5		0.4	[39]
Human osteosarcoma cell line MG63	2.38	6		[40]
Human coronary artery endothelial cells – Human aortic smooth muscle cells – Human aortic adventitial fibroblasts	5			[41]
Endothelial cells – Smooth muscle cells		4	0.135	[42]
Pulmonary artery endothelial cells – Smooth muscle cells	3		0.62	[43]
Endothelial cells	3		0.65 – 1	[44]
Human umbilical vein endothelial cells	3		0.65 – 0.68	[45]
Human dermal neonatal fibroblasts – Human umbilical vein endothelial cells	0.4855	0.67		[46]
Human glioma cell line U118 – Human glioma stem cells GSC23	0.47	0.867		[47]

of microbeads on most surface area of the hollow channel and some microbeads in the HUVEC vessel have not flowed or flowed relatively slowly. These not moving or slow-moving microbeads were supposed to attach to the channel surface like the flow-enhanced cell adhesion[48-50]. The hollow channel was made continuously and uniformly by the microfluidic laminar flow device. However, the HUVEC vessel was formulated by HUVEC's natural tendency so that its structure would be much more complex and variable.

The HUVECs in the flowing condition have elongated much more in their shapes and aligned much more with each other (**Figure 9**) than into two other conditions. ECs recognize minor variations in the direction, magnitude, and shear stress and respond by directing vasculature remodeling[51,52]. ECs are continuously contacted *in vivo* to shear stress from blood flow to maintain vascular homeostasis[53,54]. Mechanical stimulation is an integral component of tissue development, in which it can distinctly influence cell behavior by inducing morphological and transcriptional changes[55,56]. ECs tend to respond to fluid shear stress to minimize resistance, modifying the ECs phenotype[57,58]. ECs align and elongate due to the mechanically affected distribution of cytoskeleton proteins when shear stress occurs with the perfusion process[59-61]. Besides, ECs become more elongated with long-term culture related to the stable cell-cell junction and higher motility capacity[62,63]. Interestingly, the lumen structure could be more expanded than the initial status based on the perfused process through the HUVECs core with hydrodynamic forces from the medium flow.

The cell viability decreased from day 1 to day 10 in two non-flowing conditions. As their viability decreased, their morphology was contracted and variably distributed. It was known that cell apoptosis is related to cell shrinkage as well as cell migration[64-66]. The healthy HUVECs could migrate, and this could affect the scaffold shrinkage. Sailon *et al.* demonstrated that a well-designed media supply tool could culture up to 6 mm thick scaffold[67]. Considering the long-term viability of our flowing media inside, the methodology of our laboratory made connecting device could be a good option for three-dimensional thick scaffold culture.

The cells in the flowing condition showed the most active angiogenesis during all the time points (**Figure 12**). All the sprouting of the flowing condition were toward the hollow channel, which flowed the additional GFs media (**Figure 12C**). It was supposed that the concentration gradient from the hollow channel (**Figure 7**) affected the sprouting directionality of the flowing condition. None of the sprouting reached the hollow channel (**Figure 12A-C**). Two reasons are suspected for this not reaching phenomenon. First, the outer shell material (mixture of gelatin and alginate) between the two vasculatures inside the formulated scaffold could hinder sprouting. Because animal cells do not produce endogenous alginases to enzymatically degrade alginate scaffolds[68], the sprouting from the

HUVEC vessel could not invade into the outer shell. The second reason might be the additional GF stimulating time. The flowing and soaking conditions exhibited the sprouting length's increasing tendency up to day 10, the last observation day. Considering this inclination, longer additional GF stimulating time could grow the sprouting up to the hollow channel.

All the sprouting of the obstructing condition have disappeared at day 10, different from the other two culture conditions. Melly *et al.* also mentioned that the new vessels are unstable and depend on continued GFs stimulation until 4 weeks[69]. If the expression is lost before this time, sprouting will regress and disappear[69]. Shin *et al.* noticed that direct tip cell connections principally regulated the life cycle of stalk cells[70]. Stalk cells became disorganized, regressed, and finally disappeared with the disconnection between stalk cells and tip cells, independent of the GF gradient type[70]. Considering these reports, the low diffusion in the obstructing condition might cause the sprouting disappearance at day 10.

5. Conclusion

The two-vasculature-embedded scaffold was formulated using our two-core-embedded device. One channel developed into the HUVEC vessel, and the other channel was utilized to flowing culture media. This culture flowing through the near hollow channel enhanced HUVECs' behavior, especially angiogenic sprouting. Our scaffold and device have the potential to apply for vascular investigation, three-dimensional bioprinting, and drug discovery.

Funding

This work was supported by the Ministry of Science and ICT, Republic of Korea (NRF-2020R1F1A1075779) and by the Practical technology development medical microrobot Program (R&D Center for Practical Medical Microrobot Platform, HI19C0642) funded by the Ministry of Health and Welfare (MOHW, Republic of Korea) and the Korea Health Industry Development Institute (KHIDI, Republic of Korea), and supported by Korean Medical Device Development Fund (KMDF PR 20210527 0006-2021-01), Republic of Korea.

Conflict of interest

The authors have no conflicts of interest to declare.

Author contributions

K.K.I. guided and supervised the project. N.C.T. and D.V.T. designed and supervised the experiments. N.C.T, D.V.T, H.C.H., and K.K.I. conducted experiments and contributed intellectually to the scientific design of the project.

References

1. Vajda J, Milojević M, Maver U, *et al.*, 2021, Microvascular Tissue Engineering a Review. *Biomedicines*, 9:589. https://doi.org/10.3390/biomedicines9060589
2. Meng X, *et al.* Rebuilding the Vascular Network: *In Vivo* and *In Vitro* Approaches. *Front Cell Dev Biol Rev*, 9:639299. https://doi.org/10.3389/fcell.2021.639299
3. Sarker MD, Naghieh S, Sharma NK, *et al.*, 2018, 3D Biofabrication of Vascular Networks for Tissue Regeneration: A Report on Recent Advances. *J Pharm Anal*, 8:277–96. https://doi.org/10.1016/j.jpha.2018.08.005
4. Bae H, Puranik AS, Gauvin R, *et al.*, 2012, Building Vascular Networks. *Sci Transl Med*, 4:160ps23. https://doi.org/10.1126/scitranslmed.3003688
5. Torre-Muruzabal A, Daelemans L, Van Assche G, *et al.*, 2016, Creation of a Nanovascular Network by Electrospun Sacrificial Nanofibers for Self-healing Applications and its Effect on the Flexural Properties of the Bulk Material. *Polymer Testing*, 54:78–83. https://doi.org/10.1016/j.polymertesting.2016.06.026
6. Kinstlinger IS, Saxton SH, Calderon GA, *et al.*, 2020, Generation of Model Tissues with Dendritic Vascular Networks Via Sacrificial Laser-sintered Carbohydrate Templates. *Nat Biomed Eng*, 4:916–32. https://doi.org/10.1038/s41551-020-0566-1
7. Arakawa CK, Badeau BA, Zheng Y, *et al.*, 2017, Multicellular Vascularized Engineered Tissues through User-Programmable Biomaterial Photodegradation. *Adv Mater*, 29:1703156. https://doi.org/10.1002/adma.201703156
8. Duong VT, Dang TT, Nguyen T, *et al.*, 2018, Cell Attachment on Inside-Outside Surface and Cell Encapsulation in Wall of Microscopic Tubular Scaffolds for Vascular Tissue-Like Formation. Hawaii, USA: EMBC. https://doi.org/10.1109/EMBC.2018.8513248
9. Duong VT, Koo K, 2019, Over-Five-Millimeter Diameter Alginate-Collagen Endothelialized Tubular Scaffold Formation. Basel, Switzerland: MicroTAS.
10. Duong VT, Jong PK, Kim K, *et al.*, 2018, Three-dimensional Bio-printing Technique: Trend and Potential for High Volume Implantable Tissue Generation. *Korean Soc Med Biomed Eng*, 39:188–207. https://doi.org/10.9718/JBER.2018.39.5.188
11. Koo KI, Lenshof A, Huong LT, *et al.*, 2021, Acoustic Cell Patterning in Hydrogel for Three-Dimensional Cell Network Formation. *Micromachines*, 12:3. https://doi.org/10.3390/mi12010003

12. Sekine H, Okano T, 2021, Capillary Networks for Bio-Artificial Three-Dimensional Tissues Fabricated Using Cell Sheet Based Tissue Engineering. *Int J Mol Sci*, 22:92. https://doi.org/10.3390/ijms22010092
13. Bertlein S, Hikimoto D, Hochleitner G, *et al.*, 2018, Development of Endothelial Cell Networks in 3D Tissues by Combination of Melt Electrospinning Writing with Cell-Accumulation Technology. *Small*, 14:1701521. https://doi.org/10.1002/smll.201701521
14. Wang Z, Mithieux SM, Weiss AS, 2019, Fabrication Techniques for Vascular and Vascularized Tissue Engineering. *Adv Healthc Mater*, 8:1900742. https://doi.org/10.1002/adhm.201900742
15. van Duinen V, Zhu D, Ramakers C, *et al.*, 2019, Perfused 3D Angiogenic Sprouting in a High-throughput *In Vitro* Platform. *Angiogenesis*, 22:157–65. https://doi.org/10.1007/s10456-018-9647-0
16. Del Amo C, Borau C, Gutiérrez R, *et al.*, 2016, Quantification of Angiogenic Sprouting under Different Growth Factors in a Microfluidic Platform. *J Biomech*, 49:1340–6. https://doi.org/10.1016/j.jbiomech.2015.10.026
17. Farahat WA, Wood LB, Zervantonakis IK, *et al.*, 2012, Ensemble Analysis of Angiogenic Growth in Three-dimensional Microfluidic Cell Cultures. *PLoS One*, 7:e37333. https://doi.org/10.1371/journal.pone.0037333
18. Duong VT, Dang TT, Hwang CH, *et al.*, 2020, Coaxial Printing of Double-layered and Free-standing Blood Vessel Analogues without Ultraviolet Illumination for High-volume Vascularised Tissue. *Biofabrication*, 12:045033. https://doi.org/10.1088/1758-5090/abafc6
19. Gao G, Park JY, Kim BS, *et al.*, 2018, Coaxial Cell Printing of Freestanding, Perfusable, and Functional *In Vitro* Vascular Models for Recapitulation of Native Vascular Endothelium Pathophysiology. *Adv Healthc Mater*, 7:e1801102. https://doi.org/10.1002/adhm.201801102
20. Duong VT, Nguyen T, Phan L, *et al.*, 2018, Multi-Lumen Tubular Calcium-Alginate Cell-Laden Scaffold Formation for 3D Bioprinting. Taiwan: Presented at the MicroTAS, Kaohsiung, Taiwan.
21. Nguyen DH, Stapleton SC, Yang MT, *et al.*, 2013, Biomimetic Model to Reconstitute Angiogenic Sprouting Morphogenesis *In Vitro*. *Proc Natl Acad Sci U S A*, 110:6712–7. https://doi.org/10.1073/pnas.1221526110
22. Iruela-Arispe ML, Davis GE, 2009, Cellular and Molecular Mechanisms of Vascular Lumen Formation. *Dev Cell*, 16:222–31. https://doi.org/10.1016/j.devcel.2009.01.013
23. Sugihara K, Yamaguchi Y, Usui A, *et al.*, "A New Perfusion Culture Method with a Self-organized Capillary Network. *PLoS One*, 15:e0240552. https://doi.org/10.1371/journal.pone.0240552
24. Duong VT, Dang TT, Kim JP, *et al.*, 2019, Twelve-day Medium Pumping into Tubular Cell-laden Scaffold Using a Lab-made PDMS Connector. *Eur Cell Mater*, 38:1–13. https://doi.org/10.22203/eCM.v038a01
25. Duong VT, Nguyen T, Choi M, *et al.*, 2017, Twenty-Day Culturing of Tubular Scaffolds Using Micro-Connector with HeartMimicking Medium Pumping for Blood Vessel Modeling. Georgia, USA: MicroTAS Georgia, USA.
26. Fisher AB, Chien S, Barakat AI, *et al.*, 2001, Endothelial Cellular Response to Altered Shear Stress. *Am J Physiol Lung Cell Mol Physiol*, 281:L529–33. https://doi.org/10.1152/ajplung.2001.281.3.L529
27. Sarker B, Singh R, Silva R, *et al.*, 2014, Evaluation of Fibroblasts Adhesion and Proliferation on Alginate-gelatin Crosslinked Hydrogel. *PLoS One*, 9:e107952. https://doi.org/10.1371/journal.pone.0107952
28. Sarker B, Papageorgiou DG, Silva R, *et al.*, 2014, Fabrication of Alginate-gelatin Crosslinked Hydrogel Microcapsules and Evaluation of the Microstructure and Physico-chemical Properties. *J Mater Chem B*, 2:1470–82. https://doi.org/10.1039/C3TB21509A
29. Jiang T, Munguia-Lopez J, Flores-Torres S, *et al.*, 2018, Bioprintable Alginate/Gelatin Hydrogel 3D *In Vitro* Model Systems Induce Cell Spheroid Formation. *J Vis Exp*, 137:57826. https://doi.org/10.3791/57826
30. Rouwkema J, Koopman B, Blitterswijk C, *et al.*, 2010, Supply of Nutrients to Cells in Engineered Tissues. *Biotechnol Genet Eng Rev*, 26:163–78. https://doi.org/10.5661/bger-26-163
31. Krogh A, 1919, The Supply of Oxygen to the Tissues and the Regulation of the Capillary Circulation. *J Physiol*, 52:457–74. https://doi.org/10.1113/jphysiol.1919.sp001844
32. Place TL, Domann FE, Case AJ, 2017, Limitations of Oxygen Delivery to Cells in Culture: An Underappreciated Problem in Basic and Translational Research. *Free Radic Biol Med*, 113:311–22. https://doi.org/10.1016/j.freeradbiomed.2017.10.003
33. Cao X, Maharjan S, Ashfaq R, *et al.*, 2021, Bioprinting of Small-Diameter Blood Vessels. *Engineering*, 7:832–44. https://doi.org/10.1016/j.eng.2020.03.019
34. Yan J, Liu X, Liu J, *et al.*, 2021, A Dual-layer Cell-laden

Tubular Scaffold for Bile Duct Regeneration. *Mater Des*, 212:110229.
https://doi.org/10.1016/j.matdes.2021.110229

35. Bombaldi de Souza FC, Camasão DB, Bombaldi de Souza RF, *et al.*, 2020, A Simple and Effective Approach to Produce Tubular Polysaccharide-based Hydrogel Scaffolds. *J Appl Polym Sci*, 137:48510.
https://doi.org/10.1002/app.48510
36. Akkouch A, Yu Y, Ozbolat IT, 2015, Microfabrication of Scaffold-free Tissue Strands for Three-dimensional Tissue Engineering. *Biofabrication*, 7:031002.
https://doi.org/10.1088/1758-5090/7/3/031002
37. Fayol D, Le Visage C, Ino J, *et al.*, 2013, Design of Biomimetic Vascular Grafts with Magnetic Endothelial Patterning. *Cell Transplantation*, 22:2105–18.
https://doi.org/10.3727/096368912x661300
38. Ju YM, Ahn H, Arenas-Herrera J, *et al.*, 2017, Electrospun Vascular Scaffold for Cellularized Small Diameter Blood Vessels: A Preclinical Large Animal Study. *Acta Biomater*, 59:58–67.
https://doi.org/10.1016/j.actbio.2017.06.027
39. Daum R, Visaser D, Wild C, *et al.*, 2020, Fibronectin Adsorption on Electrospun Synthetic Vascular Grafts Attracts Endothelial Progenitor Cells and Promotes Endothelialization in Dynamic *In Vitro* Culture. *Cells*, 9:778.
https://doi.org/10.3390/cells9030778
40. Hossain KM, Zhu C, Felfel RM, *et al.*, 2015, Tubular Scaffold with Shape Recovery Effect for Cell Guide Applications. *J Funct Biomater*, 6:564–84.
https://doi.org/10.3390/jfb6030564
41. Alessandrino A, *et al.*, 2019, Three-Layered Silk Fibroin Tubular Scaffold for the Repair and Regeneration of Small Caliber Blood Vessels: From Design to *In Vivo* Pilot Tests. *Front Bioeng Biotechnol*, 7:356.
https://doi.org/10.3389/fbioe.2019.00356
42. Li MX, Li L, Zhou SY, *et al.*, 2021, A Biomimetic Orthogonal-bilayer Tubular Scaffold for the Co-culture of Endothelial Cells and Smooth Muscle Cells. *RSC Adv*, 11:31783–90.
https://doi.org/10.1039/D1RA04472A
43. Niu Y, Galluzzi M, 2021, Hyaluronic Acid/Collagen Nanofiber Tubular Scaffolds Support Endothelial Cell Proliferation, Phenotypic Shape and Endothelialization. *Nanomaterials*, 11:2334.
https://doi.org/10.3390/nano11092334
44. Niu Y, Galluzzi M, Fu M, *et al.*, 2021, *In Vivo* Performance of Electrospun Tubular Hyaluronic Acid/Collagen Nanofibrous Scaffolds for Vascular Reconstruction in the Rabbit Model. *J Nanobiotechnol*, 19:349.
https://doi.org/10.1186/s12951-021-01091-0
45. Hu Q, Su C, Zeng Z, *et al.*, 2020, Fabrication of Multilayer Tubular Scaffolds with Aligned Nanofibers to Guide the Growth of Endothelial Cells. *J Biomater Appl*, 35:553–66.
https://doi.org/10.1177/0885328220935090
46. Hong S, Kim JS, Jung B, *et al.*, 2019, Coaxial Bioprinting of Cell-laden Vascular Constructs Using a Gelatin-Tyramine Bioink. *Biomater Sci*, 7:4578–87.
https://doi.org/10.1039/C8BM00618K
47. Wang X, Li X, Dai X, *et al.*, 2018, Coaxial Extrusion Bioprinted Shell-core Hydrogel Microfibers Mimic Glioma Microenvironment and Enhance the Drug Resistance of Cancer Cells. *Colloids Surf B Biointerfaces*, 171:291–9.
https://doi.org/10.1016/j.colsurfb.2018.07.042
48. Abkarian M, Viallat A, 2005, Dynamics of Vesicles in a Wall-Bounded Shear Flow. *Biophys J*, 89:1055–66.
https://doi.org/10.1529/biophysj.104.056036
49. Zhu C, Yago T, Lou J, *et al.*, 2008, Mechanisms for Flow-enhanced Cell Adhesion. *Ann Biomed Eng*, 36:604–21.
https://doi.org/10.1007/s10439-008-9464-5
50. Park S, Joo YK, Chen Y, 2018, Dynamic Adhesion Characterization of Cancer Cells under Blood Flow-mimetic Conditions: Effects of Cell Shape and Orientation on Drag Force. *Microfluid Nanofluid*, 22:108.
https://doi.org/10.1007/s10404-018-2132-7
51. Roux E, Bougaran P, Dufourcq P, *et al.*, 2020, Fluid Shear Stress Sensing by the Endothelial Layer. *Front Physiol*, 11:861–1.
https://doi.org/10.3389/fphys.2020.00861
52. del Álamo JC, Norwich GN, Li YS, *et al.*, 2008, Anisotropic Rheology and Directional Mechanotransduction in Vascular Endothelial Cells. *Proc Natl Acad Sci*, 105:15411–6.
https://doi.org/10.1073/pnas.0804573105
53. Krüger-Genge A, Blocki A, Franke RP, *et al.*, 2019, Vascular Endothelial Cell Biology: An Update. *Int J Mol Sci*, 20:4411.
https://doi.org/10.3390/ijms20184411
54. Chistiakov DA, Orekhov AN, Bobryshev YV, 2017, Effects of Shear Stress on Endothelial Cells: Go with the Flow. *Acta Physiologica*, 219:382–408.
https://doi.org/10.1111/apha.12725.
55. Malek AM, Izumo S, 1996, Mechanism of Endothelial Cell Shape Change and Cytoskeletal Remodeling in Response to Fluid Shear Stress. *J Cell Sci*, 109 Pt 4:713–26.
56. Ballermann BJ, Dardik A, Eng E, *et al.*, 1998, Shear Stress and the Endothelium. *Kidney Int*, 54:S100–8.
https://doi.org/10.1046/j.1523-1755.1998.06720.x

57. Tsuji-Tamura K, Ogawa M, 2018, Morphology Regulation in Vascular Endothelial Cells. *Inflamm Regen*, 38:25. https://doi.org/10.1186/s41232-018-0083-8
58. Bai C, Hou L, Zhang M, *et al.*, 2012, Characterization of Vascular Endothelial Progenitor Cells from Chicken Bone Marrow. *BMC Vet Res*, 8:54. https://doi.org/10.1186/1746-6148-8-54
59. Fletcher DA, Mullins RD, 2010, Cell Mechanics and the Cytoskeleton. *Nature*, 463:485–92. https://doi.org/10.1038/nature08908
60. Inglebert M, Mullins RD, 2020, The Effect of Shear Stress Reduction on Endothelial Cells: A Microfluidic Study of the Actin Cytoskeleton. *Biomicrofluidics*, 14:024115. https://doi.org/10.1063/1.5143391
61. Osborn EA, Rabodzey A, Dewey JC, *et al.*, 2006, Endothelial Actin Cytoskeleton Remodeling during Mechanostimulation with Fluid Shear Stress. *Am J Physiol Cell Physiol*, 290:C444–52. https://doi.org/10.1152/ajpcell.00218.2005
62. Pasini A, *et al.*, 2021, Perfusion Flow Enhances Viability and Migratory Phenotype in 3D-Cultured Breast Cancer Cells. *Ann Biomed Eng*, 49:2103-13. https://doi.org/10.1007/s10439-021-02727-w
63. Cavey M, Lecuit T, 2009, Molecular Bases of Cell-cell Junctions Stability and Dynamics. *Cold Spring Harb Perspect Biol*, 1:a002998. https://doi.org/10.1101/cshperspect.a002998
64. Coffman CR, 2003, Cell Migration and Programmed Cell Death of *Drosophila* Germ Cells. *Ann N Y Acad Sci*, 995:117–26. https://doi.org/10.1111/j.1749-6632.2003.tb03215.x
65. Ye F, Song J, Wang Y, *et al.*, 2018, Proliferation Potential-Related Protein Promotes the Esophageal Cancer Cell Proliferation, Migration and Suppresses Apoptosis by Mediating the Expression of p53 and Interleukin-17. *Pathobiology*, 85:322–31. https://doi.org/10.1159/000492393
66. Gorelick-Ashkenazi A, Weiss R, Sapozhnikov L, *et al.*, 2018, Caspases Maintain Tissue Integrity by an Apoptosis-independent Inhibition of Cell Migration and Invasion. *Nat Commun*, 9:2806. https://doi.org/10.1038/s41467-018-05204-6
67. Sailon AM, Allori AC, Davidson EH, *et al.*, 2009, A Novel Flow-Perfusion Bioreactor Supports 3D Dynamic Cell Culture. *J Biomed Biotechnol*, 2009:873816. https://doi.org/10.1155/2009/873816
68. Ashton RS, Banerjee A, Punyani S, *et al.*, 2007, Scaffolds Based on Degradable Alginate Hydrogels and Poly(Lactide-co-glycolide) Microspheres for Stem Cell Culture. *Biomaterials*, 28:5518–25. https://doi.org/10.1016/j.biomaterials.2007.08.038
69. Melly L, Boccardo S, Eckstein F, *et al.*, 2012, Cell and Gene Therapy Approaches for Cardiac Vascularization. *Cells*, 1:961–75. https://doi.org/10.3390/cells1040961
70. Shin Y, Jeon JS, Han S, *et al.*, 2011, *In Vitro* 3D Collective Sprouting Angiogenesis under Orchestrated ANG-1 and VEGF Gradients. *Lab Chip*, 11:2175–81. https://doi.org/10.1039/C1LC20039A

Publisher's note